Proc. Natl. Acad. Sci. USA
Vol. 89, pp. 2995–2999, April 1992
Biophysics

Theory of hydrophobicity: Transient cavities in molecular liquids

(solubilities/scaled particle model/cavity size distributions/cavity formation work/surface tension)

LAWRENCE R. PRATT† AND ANDREW POHORILLE‡§

†Los Alamos National Laboratory, Los Alamos, NM 87545; ‡Department of Chemistry, University of California, Berkeley, CA 94720; and §National Aeronautics and Space Administration-Ames Research Center, Moffett Field, CA 94035

Communicated by Frank H. Stillinger, November 25, 1991 (received for review October 8, 1991)

ABSTRACT **Observation of the size distribution of transient cavities in computer simulations of water, *n*-hexane, and *n*-dodecane under benchtop conditions shows that the sizes of cavities are more sharply defined in liquid water but the most-probable-size cavities are about the same size in each of these liquids. The calculated solvent atomic density in contact with these cavities shows that water applies more force per unit area of cavity surface than do the hydrocarbon liquids. This contact density, or "squeezing" force, reaches a maximum near cavity diameters of 2.4 Å. The results for liquid water are compared to the predictions of simple theories and, in addition, to results for a reference simple liquid. The numerical data for water at a range of temperatures are analyzed to extract a surface free energy contribution to the work of formation of atomic-size cavities. Comparison with the liquid–vapor interfacial tensions of the model liquids studied here indicates that the surface free energies extracted for atomic-size cavities cannot be accurately identified with the macroscopic surface tensions of the systems.**

The solubilities of inert gases in water—hydrophobic solubilities—are the subject of current interest because of their relevance to our understanding of the molecular assembly of large-scale structures in aqueous solutions (1–3). The folding or association of proteins (4–6) and the formation of micelles and membranes (7–9) are examples of such assembly processes.

A central quantity in theories of hydrophobic solubilities is the quasi-static work required to open in the solvent a cavity of sufficient size to accommodate the solute (10). Recently, it has been demonstrated that this cavity formation work can be obtained efficiently for spherical atomic-size cavities by study of transient cavities observed in molecular dynamics simulations of the neat solvents (11). Comparison of those quantities for aqueous and nonaqueous solvents provides direct insight into the molecular mechanisms responsible for hydrophobic solubilities. Additionally, those data should provide the basis for more accurate simple theories (1, 12–16) that might be applicable to the problems indicated above.

That experimental solubilities of inert gases are typically greater in organic solvents than in water suggests that the likelihood of finding a cavity of atomic size is greater in organic liquids. However, the fractional free volume is larger for water than for typical organic solvents—i.e., typical organic liquids are denser than liquid water when viewed in terms of the packing fraction. In the context of a simple solubility model, the scaled particle model (12–14), those facts have suggested that the relative smallness of interstitial holes in liquid water is not chiefly due to specific intermolecular correlations of this unique solvent but instead is mostly due to the relatively small size of the water molecule (17, 18) and, furthermore, that the free volume is distributed in smaller packets for water (11). The primary objective of this study was to obtain numerically exact results that permit a direct test of the theoretical solubility models that might lead to such interesting physical conclusions.

The publication costs of this article were defrayed in part by page charge payment. This article must therefore be hereby marked "*advertisement*" in accordance with 18 U.S.C. §1734 solely to indicate this fact.

OBJECTIVES AND METHODS

Several related mathematical quantities are especially significant to the study of transient cavities in liquids and to the development of the scaled particle treatments. The first such quantity is the insertion probability, $p(R)$. It is defined as the likelihood that a hard sphere solute of radius R could be located at an arbitrary point within the liquid without overlap with the van der Waals volume of any solvent molecule. If V_R denotes the average volume accessible to such a solute, then

$$p(R) \equiv \frac{V_R}{V}, \qquad [1]$$

where V is the volume of the solvent.

The second quantity of interest, $p_m(R)$, is related to $p(R)$ by

$$p(R) = \int_R^\infty p_m(R')dR' \qquad [2]$$

or, conversely,

$$p_m(R) = -\frac{dp(R)}{dR}. \qquad [3]$$

Thus, $p_m(R)dR$ is the probability that the *largest* hard sphere solute that could be inserted at a randomly chosen point would have a radius within dR of R.

The present study will be limited to cases where the solvent molecules are represented as a collection of spherical interaction sites of one kind only. The extension to solvents composed of sites of several different types does not cause any conceptual complications (11). A van der Waals radius, R_S, of the solvent exclusion spheres must be given in order to calculate $p(R)$. For example, we typically consider $R_S \approx 1.35$ Å for water. However, the geometric problem of finding whether a hard sphere solute at a particular location is outside the van der Waals excluded volume depends only on the parameter $\lambda = R + R_S$ with $\lambda \geq 0$. Thus, if the results for a particular value of R_S are available for a range of R extending down to $-R_S$, results for other values of R_S can be obtained by a simple translation of the R axis (19, 20). Furthermore, results displayed as a function of λ alone are independent of R_S. The significance of negative values of the van der Waals radius R in the general scaled particle approach has been long appreciated. For the particular context of hydrophobic solubilities, this point was discussed in footnote 33 of ref. 11 where the connection of $p_m(R)$ with the nearest-neighbor distribution was emphasized. For further discussion of this latter quantity see ref. 21.

The final definition that we need combines $p(R)$ and $p_m(R)$ to describe the conditional solvent density just outside a spherical solute. Since the present study is limited to cases where the solvent molecules are represented as a collection of spherical interactions sites of one kind only, the conditional solvent density that we seek is the density of those interaction sites. They are present in the bulk liquid with density ρ_S. Then the desired conditional, or contact, density is given as

$$\rho_S G(\lambda) = \left(\frac{1}{4\pi\lambda^2}\right)\frac{p_m(R)}{p(R)}. \quad [4]$$

Since $-k_BT\ln p(R) = \Delta\mu_R$ is the work of formation of a cavity of radius R, we obtain from Eqs. 3 and 4 that

$$k_BT\rho_S G(\lambda) = \left(\frac{1}{4\pi\lambda^2}\right)\frac{d\Delta\mu_R}{dR} \quad [5]$$

is the compressive force per unit area exerted by the solvent on the cavity whose surface area is $4\pi\lambda^2$ (15, 16, 19, 20).

The data for evaluation of these quantities are molecular configurations produced by conventional molecular dynamics calculations on the neat liquids *n*-hexane, *n*-dodecane, water, and simple model atomic liquids. Ref. 11 describes the details of the calculations and the method for obtaining insertion probabilities. The molecular dynamics trajectory of ref. 11 for 343 TIP4P water molecules at temperature of 300 K and density 1 g/cm^3 was extended to 2 ns and the number of gridpoints was increased to 400,000 for each of the 8000 configurations considered. In addition, we have augmented this data to check on the magnitude of system size corrections by performing calculations on 1000 TIP4P water molecules under the same thermodynamic conditions. Four thousand configurations chosen uniformly from 0.5-ns molecular dynamics trajectory were analyzed by inserting 800,000 gridpoints in each configuration. Fig. 1 compares the $G(\lambda)$ obtained for the two different system sizes. The differences are insignificant for $\lambda < 2.0$ Å and modest for 2.0 Å $\leq \lambda \leq$ 3.5 Å.

A distinct but related issue of sensitivity of these results to system sizes derives from the following physical argument (22). When the formation of a cavity of substantial size is observed, the surrounding fluid must be somewhat compressed because the molecular dynamics calculations imposed a specific constant volume, V. If the observed cavity is about the size of one molecule, then the density of the surrounding fluid must be larger by approximately $1/V$. If the volume were very large, the effect of the constant volume constraint would not be significant. For 343 water molecules we checked the sensitivity of $G(\lambda)$ to a change in density of this magnitude by carrying out calculations in which the solvent density was decreased by $1/V$. The comparison in Fig. 1 shows that for this system size such a density change is not significant for $\lambda < 3.0$ Å.

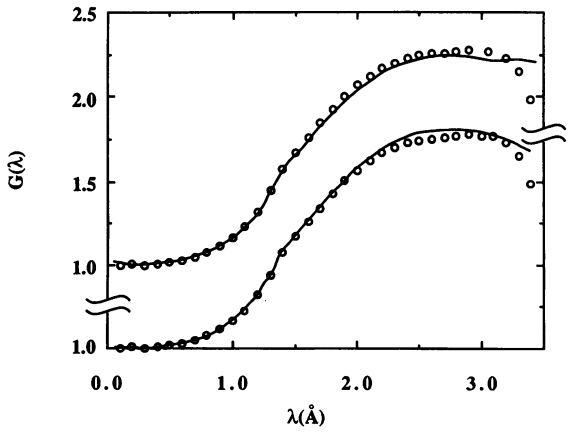

FIG. 1. The lower results test the effects of system size for the contact correlation function $G(\lambda)$ of TIP4P water at 300 K and the normal density. The circles are the molecular dynamics results for a system of 343 water molecules. The line is the same quantity for a system size of 1000 molecules. The upper results check the density dependence $G(\lambda)$ for 343 TIP4P water at 300 K. The circles are the results for a density of 0.996 g/cm^3; the line is the result for a density of 1.000 g/cm^3.

RESULTS

Two different comparative views of our results are instructive. In the first, we compare the cavity statistics obtained from simulated water with those for the paraffin solvents, *n*-hexane and *n*-dodecane, described as chains of spherical united atoms representing either methyl or methylene groups. The second comparison is between the results for water and the predictions of simple theories including results for a simple, nonassociated atomic liquid represented here by a suitably identified Lennard–Jones liquid.

Water vs. Oil. Fig. 2 shows $G(\lambda)$ for liquid water, *n*-hexane, and *n*-dodecane. The contact density at the surface of a hard sphere solute is lower in the hydrocarbon solvents than in water. Thus, the water more strongly squeezes the solute, thereby contributing to the driving force for its disposition into another phase. The kink in $G(\lambda)$ for the hydrocarbon liquids at $\lambda = 0.77$ Å is due to the rigid C—C bond, of length 1.54 Å. Due to the additional rigidity of C—C—C bond angles, another cusp should be expected at half the next-nearest-neighbor C—C distance. However, that cusp is substantially overlapped by three-body contributions to the excluded volume and is not apparent in the figure. (See Eq. 6 below.)

The contact density is slightly higher for *n*-hexane relative to *n*-dodecane. This can be interpreted in terms of a "screening" of the interaction between the hard sphere solute and methyl or methylene groups on the paraffin molecules. In order to drag such a group into contact with the solute, the conformations of the chain molecule must be somewhat restricted. This entails a free energy penalty. That penalty is somewhat larger for *n*-dodecane than for *n*-hexane because the chain molecule is longer.

Fig. 3 shows $p(R)$ and $p_m(R)$ for these liquids assuming typical values of R_S in each case. Note that these functions are followed down to the lower limit of their natural range $R \geq -R_S$. The contrast between water and the paraffin solvents is striking. One simple characteristic of the distributions

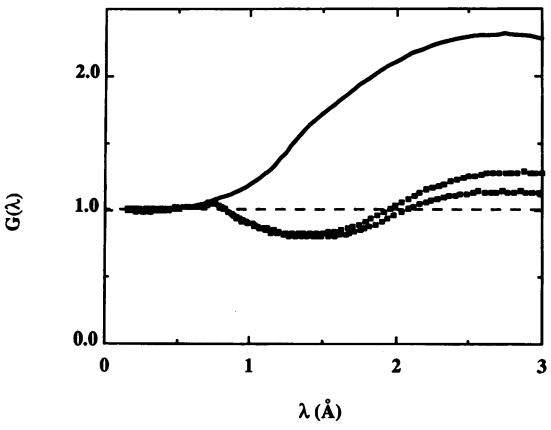

FIG. 2. $G(\lambda)$ for water, *n*-hexane, and *n*-dodecane from top to bottom, respectively, on the right side of the graph.

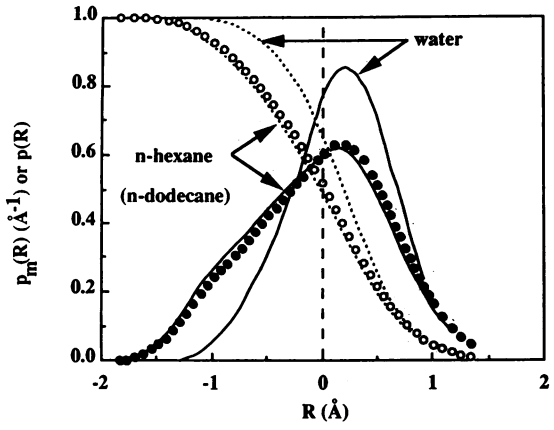

FIG. 3. Cavity size distribution functions $p(R)$ and $p_m(R)$ for water, *n*-hexane, and *n*-dodecane. Here, R_S = 1.35 Å for water molecules and 1.85 Å for methyl and methylene groups of the hydrocarbons. The results for *n*-hexane and *n*-dodecane are nearly indistinguishable for these functions. $G(\lambda)$ (Fig. 2) more sensitively distinguishes these very similar liquids.

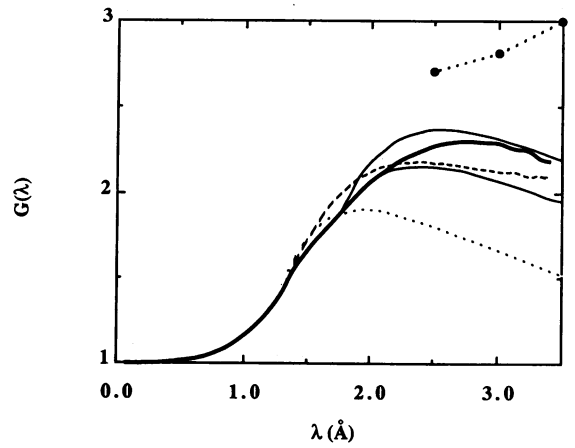

FIG. 4. $G(\lambda)$ for TIP4P water compared to theoretical results. The heavy solid curve shows the numerical results for the TIP4P model; the filled circles are the results, obtained from tabulations in the published report (12), of the integral equation approximation; the dotted line represents the scaled particle model (22); the dashed line is the result for the reference simple liquid identified in the text. The solid curves flanking the experimental results are two adaptations of the revised scaled particle model of ref. 15. The upper curve utilizes the value γ = 84 dyne/cm (1 dyne = 10 μN) in the macroscopic form Eq. 7; the lower curve uses the experimental value γ = 71.5 dyne/cm.

$p_m(R)$ is the maximum that indicates the most probable value of the van der Waals radius of the largest hard sphere that could be inserted. If this most probable value were taken as the sole indicator of the size of typical cavities that occur in these solvents, then the results of Fig. 3 would lead us to the conclusion that there is no important difference between the sizes of cavities that occur in water, *n*-hexane, and *n*-dodecane. However, the width of the size distributions $p_m(R)$ is significantly larger for the hydrocarbon liquids than for the simulated liquid water. As noted above, the widths of these distributions are independent of the radii of solvent atoms. Thus, the relative narrowness of $p_m(R)$ is a distinctive feature of liquid water. This observation provides specific support for the physical argument that cavities are more sharply defined in water than in organic solvents (11). Note particularly that the likelihood of finding an atomic-size cavity in water is less than in the liquid paraffins, in agreement with the conventional picture of the hydrophobic effect.

Comparison with Simple Theories. Here we compare the numerical results for TIP4P water with theoretical results. A conclusion that might be drawn (17, 18) from one of the "simple theories," the scaled particle model, is that hard-sphere solubilities are principally determined by the size of the solvent molecules, the packing density of the solvent, and the equation of state, but not by the specific structure of the liquid. To have a basis for testing this hypothesis, we have studied a Lennard–Jones atomic liquid, at the same number density as liquid water, for which the interaction parameters are adjusted to bring the pressure into agreement with the pressure of liquid water at 300 K and for which the intermolecular distance of closest approach is the same at that for O—O atoms in liquid water: 2.7 Å = 2 × 1.35 Å. Because the Lennard–Jones liquid is so well understood, this adjustment requires only consultation of the literature (23–25). The Lennard–Jones parameters for this reference simple liquid are ε = 272 K = 0.541 kcal/mol (1 kcal = 4.18 kJ) and σ = 2.67 Å. This reference system is rather close to liquid–vapor coexistence at $T = 0.87 \times T_c$, where T_c is the critical temperature. Since the triple temperature, T_t, is approximately $T_t = 0.56 \times T_c$ (26), this system is roughly two-thirds of the way from the triple point to the critical point. Tanaka (27) also compared cavity statistics between computer-simulated liquid water and a Lennard–Jones atomic liquid. However, he did not adjust the interatomic interactions so that the pressure of the reference liquid was the same as that for liquid water nor were the typical distances of closest molecular approach the same. For these reasons, that previous comparison is not the most useful one here. Recently, Guillot *et al.* (28) also compared cavity works between water and a hard sphere liquid. Their data confirm the results and physical argument of ref. 11.

In Fig. 4 the numerical results for $G(\lambda)$ for the TIP4P model of water are compared with results of the scaled particle model (29), two adaptations of the revised scaled particle model (15), an integral equation theory (16), and numerical results for the reference simple liquid. These comparisons provide a more sensitive test of statistical mechanical solubility models than does the comparison of cavity works alone.

Fig. 4 shows that the integral equation $G(\lambda)$ is significantly too high. We associate the errors of the integral equation results with the fact that the integral equation approximation is not expected to reproduce correctly the asymptotic, large cavity result $\lim_{\lambda\to\infty} G(\lambda) = \beta p/\rho$ (16). (Here p is the pressure, $\beta^{-1} = k_B T$, and $\rho = \rho_S$).

In contrast, $G(\lambda)$ from the scaled particle model is significantly too low. It might be expected that this simple model would be more accurate for the reference simple liquid than for water. It requires precisely the same parameters for both liquids and it was developed in the context of theories of simple liquids. However, as can be seen from Fig. 4, the scaled particle model cannot be regarded as an accurate theory for the reference liquid either. Nevertheless, the results of the model are qualitatively more similar to the numerically exact results for water and for the reference simple liquid than they are to $G(\lambda)$ for the hydrocarbon liquids (Fig. 2).

The two curves that represent the revised scaled particle model bracket the numerical results over the range shown. The revised scaled particle model improves on its predecessor in three important ways. The first modification improves the description of the small cavity behavior by the use of the known oxygen–oxygen pair distribution function for liquid water. This modification is based on the exact relation:

$$p(R) = 1 + \sum_{j=1} (-1)^j \left\langle \frac{n_\lambda!}{j!(n_\lambda - j)!} \right\rangle, \qquad [6]$$

where n_λ is the instantaneous number of oxygen atoms within a sphere of radius λ (15, 19, 20, 30, 31). The brackets indicate

the thermal average over configurations of the neat solvent. The $j = 2$ term in this sum can be calculated exactly if exact results are available for the oxygen–oxygen pair distribution function of the solvent.

Truncation of the series Eq. 6 after the $j = 2$ term produces a theory that is correct in a small cavity domain but incorrect for large cavities. For large λ, $G(\lambda)$ is expected to behave asymptotically as

$$G(\lambda) \sim \left(\frac{\beta p}{\rho}\right) + \left(\frac{2\beta\gamma}{\rho}\right)\lambda^{-1} - \left(\frac{4\beta\gamma\delta}{\rho}\right)\lambda^{-2} + \cdots, \quad [7]$$

where γ is the tension of the liquid–vapor interface of the pure solvent and δ describes a curvature correction (15). The second modification of the scaled particle model is the use of the measured surface tension γ to improve the large cavity behavior of $G(\lambda)$.

The final modification of the scaled particle model to achieve the revised theory is to assume that the formula

$$G(\lambda) = \left(\frac{\beta p}{\rho}\right) + \left(\frac{2\beta\gamma}{\rho}\right)\lambda^{-1} - \left(\frac{4\beta\gamma\delta}{\rho}\right)\lambda^{-2} + G_4\lambda^{-4} \quad [7']$$

is accurate for λ greater than λ^* to be specified. This formula is then required to join smoothly at λ^* with the $G(\lambda)$ calculated from Eq. 6. This requirement determines δ and G_4. The adaptations of the revised scaled particle model shown in Fig. 4 implement these ideas using the oxygen–oxygen radial distribution function for the TIP4P model of water. The three-term approximation to the series for $p(R)$ is accurately equal to our numerical results for $\lambda \leq 1.7$ Å. The revised scaled particle model results shown in Fig. 4 used $\lambda^* = 1.75$ Å as the joining point. The two different curves correspond to different values of γ that were assumed. The lower curve employs the measured tension of the water liquid–vapor interface. The higher curve adopts a value of $\gamma = 84$ dyne/cm obtained from the direct fit to Eq. 7, as discussed in the next section. Fig. 4 shows that the revised scaled particle model can be effective in describing our cavity statistics over the range shown.

The numerical results show a gentle maximum in $G(\lambda)$ for cavities $\lambda \approx 2.4$ Å. This is consistent with the conventional picture that $G(\lambda)$ should exhibit a single maximum that can be taken as the "continental divide" between a small cavity region and a large cavity region. In view of Eq. 7, the position of this maximum suggests the importance of the macroscopic, large cavity behavior for rather small solutes. In this regard we note that the work of Postma *et al.* (32) suggested that $G(\lambda)$ does not exhibit just a single local maximum. Although precisely the contact density was not calculated in that work, the published results indicate the presence of *two* local maxima, one located near $\lambda \approx 3.0$ Å and another around $\lambda \approx 4.5$ Å. Since our results extend only to $\lambda = 3.5$ Å, we are unable to verify the existence of the second maximum in this study.

The observed differences in $G(\lambda)$ between water and the reference simple liquid are due to differences between the characteristic structures of these liquids. These differences are modest but appreciable even for the small sized cavities beginning with $\lambda > 1.35$ Å. More specifically, the atomic pair correlation function for the reference liquid is different than the oxygen–oxygen function for water and, therefore, the $j = 2$ term in Eq. 6 is different for these two liquids. The importance of the correct atomic pair structure can be seen by comparison of the scaled particle model results with those of the revised scaled particle theory. The revised theory incorporates the known oxygen–oxygen pair correlation function and provides the correct $j = 2$ term of Eq. 6. This leads to significant differences in $G(\lambda)$ in the range 1.35 Å $< \lambda < \lambda^*$. But the effect of the $j = 2$ term extends beyond this range, contributing to the differences between the two theories for $\lambda^* < \lambda$.

Analysis of Cavity Surface Free Energies. The scaled particle model is known to impute improper temperature variations to the surface tension of the water liquid–vapor interface (refs. 15 and 33; table XVI of ref. 19 and supporting discussion). It is interesting to ask whether utilizing numerically exact results for $G(\lambda)$ over the same microscopic length scales would provide an accurate description of thermodynamics of that interface. Eq. 7 leads to a simple graphical analysis that addresses that question. Since the pressure is low for the thermodynamic states of interest, the constant term of Eq. 7 may be neglected. Under that assumption, a plot of $\lambda^2 G(\lambda)$ should be linear and the coefficient of the linear term determines the parameter γ.

We have performed such an analysis for $G(\lambda)$ obtained from molecular dynamics calculations on TIP4P water at four different temperatures. The primary $G(\lambda)$ results are shown in Fig. 5 and the graphical analysis is displayed in Fig. 6. Over the range covered by the data, the linearity of the curves is good.

The γ parameter extracted from least-squares fitting of a linear function to the curve $T = 303$ K of Fig. 6 is 84 dyne/cm, somewhat larger than the experimental liquid–vapor surface tension of 71 dyne/cm. The γ values obtained for the other temperatures decrease with increasing temperature more rapidly than do the experimental surface tensions so that at the highest temperature treated here the extracted γ parameter is very close to the experimental surface tension of the water liquid–vapor interface. Considering that the curves in Fig. 6 are approximately linear down to $\lambda = 1.75$ Å ($R = 0.4$ Å), it might be suggested that Eq. 7 gives a satisfactory description of $G(\lambda)$ even for cavities of subatomic sizes. However, it should be borne in mind that liquid–vapor interfacial thermodynamics was not considered in the parameterization of the TIP4P model of water; therefore, this model cannot be expected to give an accurate description of interfacial properties. Indeed, the one calculation of the liquid–vapor interfacial tension for this model (34, 35) yielded a value of about 140 dyne/cm at 325 K, quite different from the fitted γ. Furthermore, if the same analysis is applied to the results for the reference simple liquid, similarly good linearity is observed with the parameter $\gamma \approx 54$ dyne/cm. This is consistent with Fig. 4, which indicates that, over the range shown, the $G(\lambda)$ results for TIP4P water and for the reference simple liquid are not wildly dissimilar. However, numerical results for the Lennard–Jones liquid (36) and experimental results for liquid Ar (27) indicate that the liquid–vapor surface tension for the reference simple liquid should be $\gamma \approx 15$ dyne/cm.

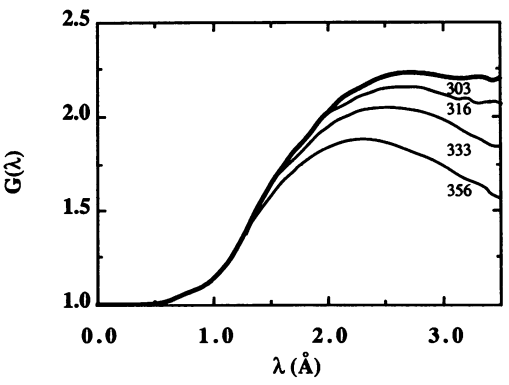

FIG. 5. Temperature dependence of $G(\lambda)$ for the TIP4P model of water at experimental densities for atmospheric pressure. The numbers labeling the four curves give the temperatures in K.

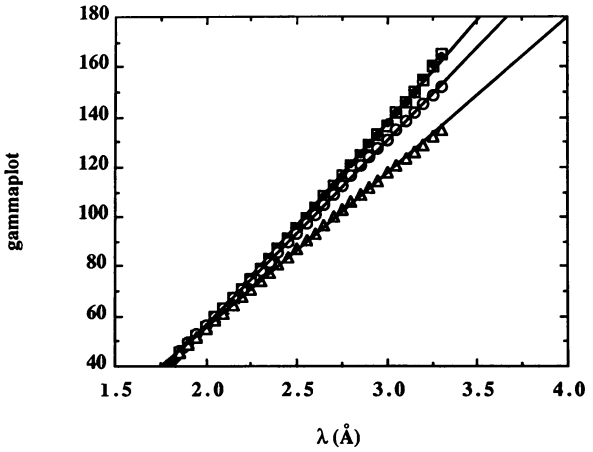

FIG. 6. Plot of $4\pi\lambda^2 G(\lambda)$ vs. λ for the results of Fig. 5. The units have been chosen so that the slopes of these curves are γ of Eq. 7 in dyne/cm. The γ values obtained from least-squares fitting of linear functions to these data are 84, 80, 74, and 62 dyne/cm from the highest to the lowest temperatures, respectively, indicated in Fig. 5.

Because of these points, we conclude that the γ parameters extracted from Fig. 6 are not accurately the liquid–vapor surface tensions for the models considered. We therefore expect that if results over a much larger range of cavity sizes were available then the slopes of the graphs of Fig. 6 would continually and gradually shift to the $\lambda \rightarrow \infty$ asymptotic behavior characteristic to a given model liquid.

CONCLUSIONS

Observation of the size distribution of transient cavities in computer simulations of water, *n*-hexane, and *n*-dodecane under benchtop conditions has shown that the most probable sizes of cavities in these liquids are similar but the distribution of cavity sizes is markedly sharper in liquid water. When the solvent atomic density in contact with these cavities was examined, it established that water applies more force per unit area of cavity surface than do the hydrocarbon liquids. This contact density, or "squeezing" force, reaches a maximum near cavity diameters of 2.4 Å. These new numerical results and analyses provide an especially stringent test of theories of hydrophobic solubilities and provide new insight into the molecular mechanisms of hydrophobic effects.

$G(\lambda)$ for liquid water was compared to the predictions of simple theories and, in addition, to results for a reference simple liquid. The integral equation results for the contact density are significantly too high and the corresponding predictions of the scaled particle model are significantly too low. The failure of the integral equation theory for these quantities is probably related to a failure of the theory to conform to the expected limit for macroscopically large cavities—i.e., the wall limit. The revised scaled particle model falls between those two sets of theoretical results and, with some adaptation, can provide an effective description of the numerical data throughout the regime of intermediate cavity sizes. The differences in $G(\lambda)$ between water and a suitable reference simple liquid, without the characteristic structure of liquid water, are slight but appreciable.

The contact density for liquid water and for the scaled particle model was further compared with the same quantity for the liquid paraffins. Over the range of atomic sizes, the behavior of $G(\lambda)$ predicted by the model is more similar to the numerical results for liquid water than it is to the results for the hydrocarbon liquids. This emphasizes that, viewed on an atomic level, the hydrocarbon liquids are strongly structured liquids.

The numerical data for water over a range of temperatures were analyzed to extract a surface free energy contribution to the work of formation of atomic-size cavities. Comparison with known results for the liquid–vapor interfacial tension of these model liquids indicated that the extracted surface free energy for cavities of atomic size cannot be accurately identified with the macroscopic surface tensions for the systems.

In view of the importance of the problems of hydrophobic solubilities, we feel that it would be useful to test available theories more extensively than has been done here. Those more searching tests should probe the sensitivity of the theories to the description of the liquid water and should analyze the solubility results over a broader range of thermodynamic conditions. For further theoretical development it would also be necessary to obtain data over a wider range of cavity sizes.

This work was supported in part by National Aeronautics and Space Administration-Ames/University of California at Berkeley Intergovernmental Personnel Exchange Agreement NCA-2 315, a National Aeronautics and Space Administration/Stanford Joint Research Initiative. L.R.P. acknowledges the hospitality of the Department of Chemistry, Stanford University, and the Planetary Biology Branch of the National Aeronautics and Space Administration's Ames Research Center. Computing resources for this work were provided in part by the Numerical Aerodynamical Simulation (NAS) Program.

1. Sharp, K., Nicholls, A., Fine, R. F. & Honig, B. (1991) *Science* **252**, 106–109.
2. Dill, K. A. (1990) *Science* **250**, 297.
3. Murphy, K. P., Privilov, P. L. & Gill, S. J. (1990) *Science* **247**, 559–561.
4. Kauzmann, W. (1959) *Adv. Protein Chem.* **14**, 1–63.
5. Edsall, J. T. & McKenzie, J. A. (1983) *Adv. Biophys.* **16**, 53–183.
6. Dill, K. A. (1990) *Biochemistry* **29**, 7133–7155.
7. Tanford, C. (1980) *Science* **200**, 1012–1018.
8. Tanford, C. (1980) *The Hydrophobic Effect* (Wiley, New York), 2nd Ed.
9. Tanford, C. (1989) *Ben Franklin Stilled the Waves* (Duke Univ. Press, Durham, NC).
10. Pollack, G. L. (1991) *Science* **251**, 1323–1330.
11. Pohorille, A. & Pratt, L. R. (1990) *J. Am. Chem. Soc.* **112**, 5066–5074.
12. Pierotti, R. A. (1965) *J. Phys. Chem.* **67**, 1840–1845.
13. Pierotti, R. A. (1965) *J. Phys. Chem.* **69**, 281–292.
14. Pierotti, R. A. (1976) *Chem. Rev.* **76**, 717–726.
15. Stillinger, F. H. (1973) *J. Solution Chem.* **2**, 141–158.
16. Pratt, L. R. & Chandler, D. (1977) *J. Chem. Phys.* **67**, 3683–3704.
17. Lee, B. (1985) *Biopolymers* **24**, 813–823.
18. Lee, B. (1991) *Biopolymers* **31**, 993–1008.
19. Reiss, H. (1965) *Adv. Chem. Phys.* **9**, 1–84.
20. Reiss, H. (1977) in *Statistical Mechanics and Statistical Methods*, ed. Landman, U. (Plenum, New York), pp. 99–140.
21. Reiss, H. & Casberg, R. V. (1974) *J. Chem. Phys.* **61**, 1107–1114.
22. Torrie, G. & Patey, G. N. (1977) *Mol. Phys.* **34**, 1623–1628.
23. Hansen, J. P. & McDonald, I. R. (1986) *Theory of Simple Liquids* (Academic, New York).
24. Verlet, L. & Weis, J.-J. (1972) *Phys. Rev.* **A5**, 939–952.
25. McDonald, I. R. & Singer, K. (1972) *Mol. Phys.* **23**, 29–40.
26. Guggenheim, E. U. (1945) *J. Chem. Phys.* **13**, 253–261.
27. Tanaka, H. (1987) *J. Chem. Phys.* **86**, 1512–1520.
28. Guillot, B., Guissani, Y. & Bratos, S. (1991) *J. Chem. Phys.* **95**, 3643–3648.
29. Lucas, M. (1976) *J. Phys. Chem.* **80**, 359–362.
30. Mayer, J. E. & Montroll, E. (1941) *J. Chem. Phys.* **9**, 2–16.
31. Stell, G. (1985) in *Studies in Statistical Mechanics*, eds. Schlesinger, M. F. & Weiss, G. H. (North-Holland, Amsterdam), Vol. 12, Chapt. 6, pp. 127–156.
32. Postma, J. P. M., Berendsen, H. J. C. & Haak, J. R. (1982) *Faraday Symp. Chem. Soc.* **17**, 55–67.
33. Ben-Naim, A. & Friedman, H. L. (1967) *J. Phys. Chem.* **71**, 448–449.
34. Wilson, M. A., Pohorille, A. & Pratt, L. R. (1987) *J. Phys. Chem.* **91**, 4873–4878.
35. Wilson, M. A., Pohorille, A. & Pratt, L. R. (1988) *J. Chem. Phys.* **88**, 3281–3285.
36. Lee, J. K., Barker, J. A. & Pound, G. M. (1974) *J. Chem. Phys.* **60**, 1976–1980.